Journal of Solid State Electrochemistry (2025) 29:4965–4972
https://doi.org/10.1007/s10008-024-05995-3

ORIGINAL PAPER

Defect chemistry of pyrochlore Pr_2O_3-ZrO_2 system: the relevant thermodynamic parameters

J. C. C. Abrantes[1] · E. Gomes[1] · A. V. Shlyakhtina[2]

Received: 28 March 2024 / Revised: 31 May 2024 / Accepted: 24 June 2024 / Published online: 5 July 2024
© The Author(s) 2024

Abstract

Materials of the system Pr_2O_3-ZrO_2, namely the $Pr_2Zr_2O_7$-based pyrochlores, have received considerable attention in the last decade, being a very interesting structure for defect chemistry because of its high solubility for various dopants, anti-site behaviour between A and B, and the multitude of possible combinations of A and B that are compatible in this type of structure. The compositions $(Pr_{2-x}Zr_x)Zr_2O_{7+x/2}$ (x = 0.15), $Pr_2Zr_2O_7$, and $Pr_2(Zr_{2-x}Pr_x)O_{7-x/2}$ (x = 0.1), were prepared in previous works through the coprecipitation method and were characterised by impedance spectroscopy as a function of the oxygen partial pressure. In the present work, a defect chemistry model is proposed, and, based on the previously obtained experimental conductivity data, the relevant thermodynamic parameters were obtained by fitting, using a non-linear optimisation numerical method. The mobility of oxygen vacancies and interstitials oxygen were accurately determined, as well as the equilibrium constant of the formation of anti-Frenkel defects. It was observed that deviations from the stoichiometry promote an increase in ionic conductivity, respectively, $1.3x10^{-4}$, $1.4x10^{-3}$ and $1.7x10^{-2}$ S/cm, for the stoichiometric, excess of Pr and excess of Zr composition. The higher value obtained for the composition with an excess of Zr^{4+}, suggests a higher interstitial oxygen mobility when compared with the oxygen vacancy mobility. It is also demonstrated that the novel applied methodology of fitting conductivity experimental data with an optimisation numerical method is suitable for determining the thermodynamically relevant parameters of defect chemistry models, allowing the prediction of material properties.

Keywords Defect chemistry · Pyrochlore · Oxygen vacancies mobility · Interstitial oxygen mobility

Introduction

It is known that for practical use in SOFCs, electrolyte oxygen ion conductivity should be at least 8.4×10^{-3} S/cm at 700 °C [1]. High oxygen ion conductivity, up to 7.4×10^{-2} S/cm at 700 °C, is offered by several solid electrolytes, such as 8YSZ, GDC ($Ce_{0.9}Gd_{0.1}O_{1.95}$), and scandium-doped ZrO_2 (ScSZ) [2–7].

The Ln_2O_3 – MO_2 (Ln = La – Gd; M = Ti, Zr, Hf) systems are of special interest because they contain not only fluorite solid solutions but also pyrochlore solid solutions, which also have high oxygen ion conductivity [8–13]. As a rule, there is a relationship between the properties of compounds and solid solutions in these systems and a pronounced tendency toward the formation of cation and anion defects as a result of order–disorder (pyrochlore-fluorite) transitions [14].

This work is focused on $Pr_2Zr_2O_7$-based pyrochlores, which have received considerable attention in the last decade. The magnetic properties of praseodymium zirconate and its solid solutions have been actively studied [15–17]. It has been found that $Pr_2Zr_2O_7$-based pyrochlores (e.g. $Pr_{2-x}Ca_xZr_{1.95}In_{0.05}O_{7+\delta}$ ($x = 0.02$)) can be used as part of solid-state sensors for NO_2 contained in industrial emissions that pollute the atmosphere [18, 19]. It is proposed to develop safe, environmentally friendly pigments ($Pr_2Zr_{2-x}Fe_xO_{7-d}$ ($x = 0$, 0.05, 0.10, 0.15, 0.20, 0.25)) based on $Pr_2Zr_2O_7$ [20]. High-activity catalysts have been discovered for the CO oxidation reaction ($Pr_2Zr_{2-x}Fe_xO_{7\pm\delta}$ ($x = 0.10$)). This catalyst provides 100% CO conversion [21]. In all cases, the strategy of acceptor doping either into one sublattice or co-doping into both cationic sublattices proved effective. For direct solid oxide fuel cells using ammonia, a cathode based on defective $Pr_2Zr_2O_7$, rich in

✉ J. C. C. Abrantes
jabrantes@estg.ipvc.pt

[1] proMetheus, Instituto Politécnico de Viana do Castelo, 4900-347 Viana Do Castelo, Portugal

[2] N.N. Semenov Federal Research Center for Chemical Physics RAS, Moscow, Russia

oxygen vacancies, has been proposed [22]. The XRD and TEC results of the pyrochlore PZO indicate that there is good chemical and physical compatibility between the PZO and the YSZ electrolyte at T ≤ 1200 °C. The SOFC using the PZO-60YSZ composite cathode exhibits higher output power than that using the commercial LSM-60YSZ composite cathode [22]. The anode-supported PZO-based SOFC yields a peak power density of 1.22 W cm^{-2} at 800 °C and 0.28 W cm^{-2} at 600 °C using H_2 as fuel [22].

In previous works [12, 13], the authors studied the temperature-dependent transport properties of pyrochlore- and fluorite-like PrZrO solid solutions in air and as a function of oxygen partial pressure. The change of the ratio Pr/Zr on $Pr_2Zr_2O_7$ is expected to promote the formation of point defect to compensate for the excess of negative or positive charge induced by the deviation from the ideal stoichiometry of this pyrochlore, with consequent changes in transport properties of this material. Particular attention has been paid to pyrochlore-like ($(Pr_{2-x}Zr_x)Zr_2O_{7+x/2}$ ($x = 0.15$), $Pr_2Zr_2O_7$ and $Pr_2(Zr_{2-x}Pr_x)O_{7-x/2}$ ($x = 0.1$)) compositions. These works compared the conductivity of the prospective material with an interstitial oxide ion conductor to that of a material with possible oxygen vacancy conductivity. Also, was investigated the effect of the Pr^{3+}/Pr^{4+} ratio on the oxygen ion transport process. Following these previous studies, the present work aims to evaluate the relevant thermodynamic parameters of this system, to allow simulations of defect concentration of each defect as a function of the temperature and oxygen partial pressure. In this way, it is possible to understand the role of each dopant on the transport properties of this material, which have not yet been investigated.

Experimental part

The experimental methods that were employed were consistent with what was presented in earlier publications [12, 13]. Using coprecipitation followed by heat treatment at 1550 °C for 4 h, we prepared pyrochlore-like PrZrO solid solutions containing 30, 33.3 and 35.5 mol % Pr_2O_3, which corresponds to the following compositions: $(Pr_{2-x}Zr_x)Zr_2O_{7+x/2}$ ($x = 0.15$), $Pr_2Zr_2O_7$, $Pr_2(Zr_{2-x}Pr_x)O_{7-x/2}$ ($x = 0.1$). For simplicity, these compositions will be referred to, respectively, by *Zr015*, *Stoich* and *Pr01*. All compositions were obtained by reverse co-precipitation (pH 11.6–11.2). The initial substances used were $PrCl_3 \cdot 6H_2O$ (99.9% TU 6–09-4773–79, Russia) and $ZrOCl_2 \cdot 8H_2O$ (99%, CHIMMED, Moscow, Russia) powders, which were dissolved in distilled water. Solution concentrations were determined gravimetrically. The concentrations of the chloride solutions were 0.09 M (Pr) and 1.085 M (Zr). Titrated praseodymium chloride and zirconium chloride solutions were added to aqueous ammonia. After the formation of light green gel-like precipitates, they were aged at room temperature for 4 h. Next, the mother liquor was decanted and the rest was centrifuged. The precipitate was washed with water to remove Cl^- ions and then dried in air for 66 h at 75 °C, which allowed it to remain light green, typical of trivalent Pr.

The dry hydroxide precursors, thus, prepared were pressed at 216–259 MPa into pellets, which were then fired at 1550 °C for 4 h.

The density of the resultant samples was determined by measuring their mass and dimensions and ranged from 85 to 90% of their X-ray density.

Total conductivity versus oxygen partial pressure data was obtained between 700 and 1000 °C, by the reoxidation method, using a mixture of 95% N_2 and 5% H_2 to reduce the oxygen partial pressure (measured by a ZrO_2 -based sensor, close to the sample). Subsequently, the gas flow was shut off and the impedance spectra measures, using a Hewlett-Packard 4284A precision LCR bridge, in the frequency range of 20 Hz to 1 MHz, were taken every 10 min until the oxygen partial pressure increased to air conditions, which took more than 6 h. In this temperature range, the spectra show only one arc, which is related to the electrode reaction process, so the interception of each spectrum with the real axis of the Nyquist plot was used to evaluate the total conductivity.

As this work objective is to find some thermodynamic parameters, to avoid some mistakes due to some sample's porosity, all conductivity data was corrected using the Bruggeman correlation [23] which is widely used in different fields, namely in calculating electrical properties [24]

DefChem - Defect Chemistry Toolbox [25] was used to generate the Brouwer-type diagrams and extract the thermodynamic parameters by fitting data obtained by experimental electrical conductivity measurements as a function of the oxygen partial pressure.

Defect chemistry model

Pyrochlore $A_2B_2O_7$ is a very interesting structure for defect chemistry studies because a large number of different possible combinations of A and B are compatible in this type of structure. There is also high solubility for different types of dopants, and the anti-site behaviour between A and B can occur.

In this work, the change of the ratio Pr/Zr on $Pr_2Zr_2O_7$ is expected to promote the formation of point defect to compensate for the excess of negative or positive charge induced by the deviation from the ideal stoichiometry of this pyrochlore, with consequent changes in transport properties of this material.

The expected point defects on the pyrochlore-type structures have already been published [26–28] and structural disorder on the oxygen sublattice can be interpreted as Frenkel defects because oxygen ions shift from regularly occupied *48f* sites into normally unoccupied *8b* sites. In addition, one must consider equilibration with the gas phase, e.g. via reduction as well as

intrinsic electron–hole generation. As praseodymium is an aliovalent ion, it is also necessary to foresee its eventual reduction.

Based on the aforementioned knowledge about the defect chemistry of this type of material, using the Kröger-Vink notation [29], the equilibrium defect reactions can be described by the following equations.

The intrinsic defects include ionic and electronic defects:

• The ionic anti-Frenkel defects

$$O_o^x \overset{K_{aF}}{\Leftrightarrow} O_i'' + V_O^{\bullet\bullet} with\ K_{aF} = \frac{[O_i''][V_O^{\bullet\bullet}]}{[o_o^x]} \tag{1}$$

• The electronic band-band transfer

$$0 \overset{K_e}{\Leftrightarrow} e' + h^{\bullet}\ with\ K_e = np \tag{2}$$

The equilibrium with the atmosphere can originate an oxygen non-stoichiometry and can be expressed by:

$$\frac{1}{2}O_2 + V_O^{\bullet\bullet} \overset{K_{\mathrm{Red}}}{\Longleftrightarrow} O_O^x + 2h^{\bullet} \text{ with } K_{\mathrm{Red}} = \frac{[O_O^x]p^2}{[V_O^{\cdot\cdot}]pO_2^{\frac{1}{2}}} \tag{3}$$

As the praseodymium ion can assume the valence Pr^{3+} and Pr^{4+}, it will also be necessary to provide for the eventual reduction of this ion to its more stable form:

$$Pr_{Pr}^x + h^{\cdot} \overset{K_{Pr}}{\Longleftrightarrow} Pr_{Pr}^{\bullet} \text{with } K_{Pr} = \frac{[Pr_{Pr}^{\bullet}]}{[Pr_{Pr}^x]p} \tag{4}$$

As we change the Pr/Zr ratio, we have to predict that the excess of one cation will occupy the lattice positions of the other cation, originating defects to compensate for the difference of charge of the two cations. The following equations are written assuming an ionic compensation mechanism. Positive oxygen vacancies formation to compensate for the negative defect of $Pr_{Zr}^{'}$, and the formation of negative oxygen interstitials to compensate for the positive $Zr_{Pr}^{\bullet}$. This ionic compensation can be changed by electronic compensation, depending on the values of the equilibrium constants in Eqs. (1), (2), (3) and (4).

The above-described charge compensations can be expressed by:

• for Pr/Zr > 1:

$$\left(1+\frac{x}{2}\right)pr_20_3 + (2-x)ZrO_2 \overset{pr_2zr_2o_7}{\Longrightarrow} 2Pr_{pr}^x + xPr_{zr}' + (2-x)\,Zr_{Zr}^x + \left(7-\frac{x}{2}\right)O_o^x + \frac{x}{2}\,V_o^{\bullet\bullet} \tag{5}$$

• for Pr/Zr < 1:

$$\left(1+\frac{x}{2}\right)pr_20_3 + (2-y)ZrO_2 \overset{pr_2zr_2o7}{\Rightarrow} (2-y)\,Pr_{Pr}^x + yZr_{Pr}^{\bullet} + 2Zr_{Zr}^x + 7O_o^x + \frac{y}{2}\,O_i^e \tag{6}$$

In order to keep the overall electroneutrality the following conditions should be satisfied:

$$2[O_i''] + [Pr'_{Zr}] + n = p + 2[V_O^{\bullet\bullet}] + [Zr_{Pr}^{\bullet}] \tag{7}$$

To draw a Brouwer-type chart, with the logarithm of the defects concentration as a function of the logarithm of the oxygen partial pressure, we need to solve the above equations, which constitute a system of nonlinear equations. To solve this complex system of equations, we used the web application DefChem [25], which solves this numerically. The use of numerical methods has the advantage of enhancing the accuracy of the defect concentration on transition zones when the diagram is solved using simplified electroneutrality conditions.

Results and discussion

A detailed structure and microstructure characterisation of all compositions under study were already reported in previous papers [12, 13], and it is highlighted that after sintering at 1550 °C all compositions present a single phase with the pyrochlore-type structure, with relative density from 85 to 90% of their X-ray density. The grain size changes between 1 and 10 µm, being about 1.5 µm for Pr01, 3.5 µm for Zr015 and 10 µm for Stoich.

Conductivity behaviour as a function of the oxygen partial pressure was measured during reoxidation by impedance spectroscopy, and depending on temperature, it is possible to identify or not the different microstructure contributions to the overall electrical conductivity, as can be seen in Fig. 1. While at 300 °C, it is possible to see the impedance arcs; at 700 °C and above, it is only possible to obtain the total conductivity, which is calculated from the impedance values near the real axis. Using this methodology, the true total conductivity (bulk + grain boundary) is obtained, avoiding electrode impedance arc interference. Furthermore, due to the higher activation energy of the grain boundary conductivity, compared with the activation energy of the bulk conductivity, it is expected that at the measurement temperatures (> 700 °C), the conductivity observed will be controlled by the bulk conductivity, making the results related to the bulk and independent of microstructural issues, namely on the grain size.

With all the data obtained from each impedance spectra, it was possible to show graphically (Fig. 2) the dependence of the total conductivity as a function of oxygen partial pressure. On this chart, it is evident the ionic plateau for all compositions and an onset of p-type conductivity for high oxygen partial pressures. It is also obvious the increase of the ionic conductivity for both nonstoichiometric compositions,

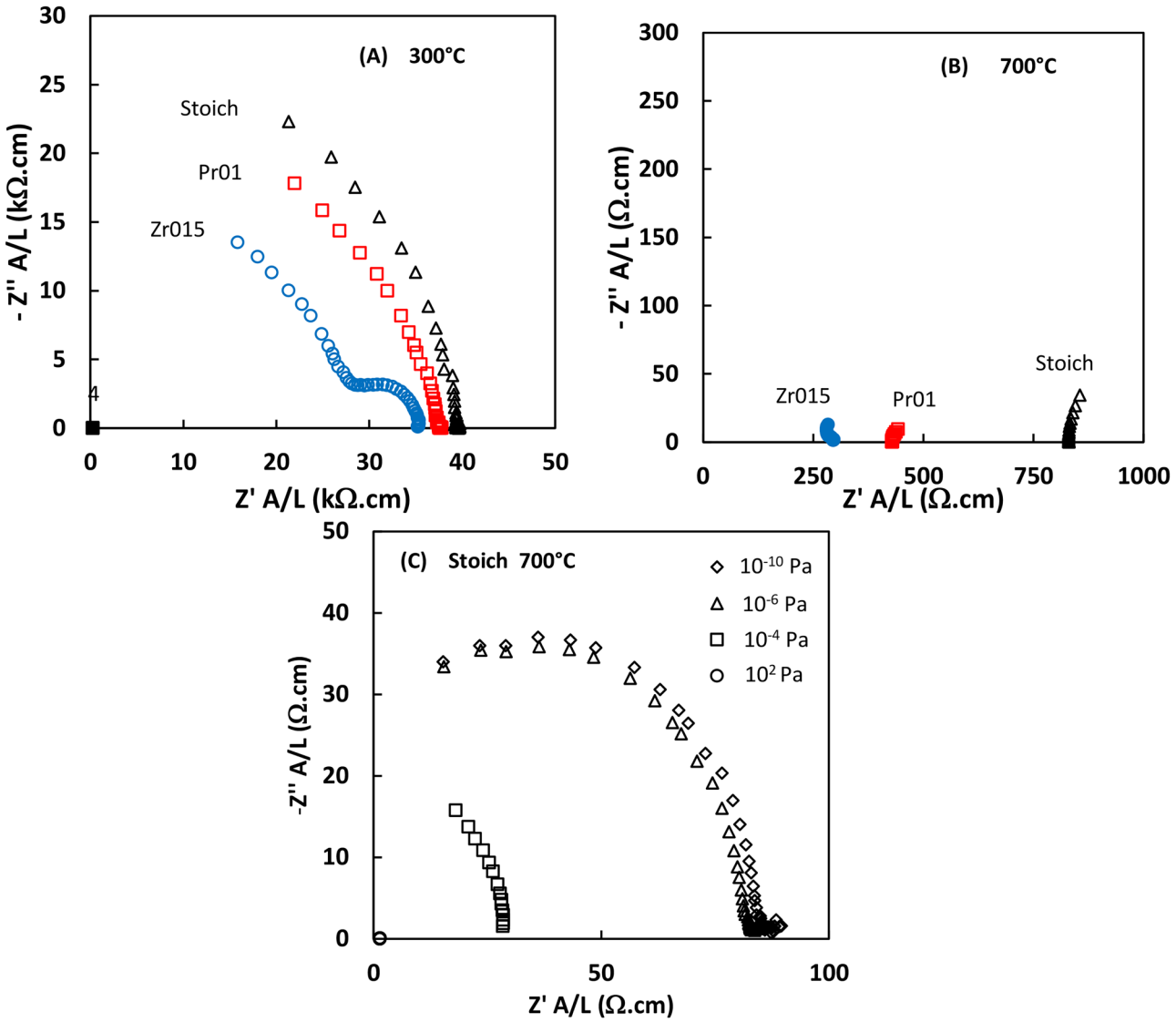

Fig. 1 Typical impedance spectra of different compositions obtained at different temperatures (**A**, **B**) and different oxygen partial pressures for the Stoich composition at 700 °C (**C**)

independently of the ratio Pr/Zr value. This result suggests that, according to the proposed defect chemistry model (Eqs. 5 and 6), the conductivity of the Pr01 composition is based on oxygen vacancies, while oxygen interstitial conductivity is present for the Zr015 composition.

According to XPS data, all prepared pyrochlore samples contain only Pr^{3+} oxidation state at room temperature [12], and as it is not expected to oxidise to Pr^{4+} at high temperatures, the defect model can be simplified because it is not necessary to include the redox equilibrium of praseodymium on Eq. (4). As it was not observed (Fig. 2) as evidence of n-type conductivity, the band-band transfer of Eq. (2) can also be discarded. So, to evaluate all defect chemistry relevant parameters of this system, it is necessary to calculate the thermodynamic data of the equilibria on Eqs. (1) and (3) and the mobility of all charged species.

Assuming the usual dependence of the electrical conductivity (σ), with the mobility (μ) and concentration ([]) of charged carrier species, and also considering that the non-stoichiometry Pr/Zr ratio controls the ionic conductivity, we can calculate the oxygen vacancies, the interstitials concentration and the corresponding ionic mobilities, using the following equations:

$$\sigma = []\mu Ze \tag{8}$$

$$\left[V_O^{\bullet\bullet}\right] = \frac{\left[Pr'_{Zr}\right]}{2} \tag{9}$$

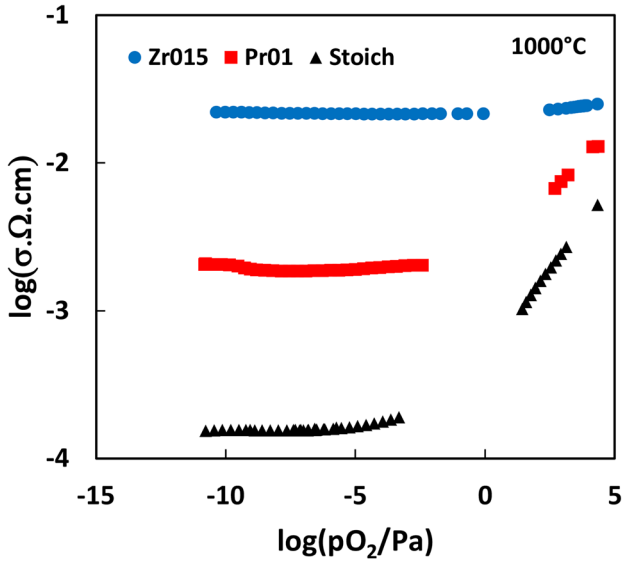

Fig. 2 Dependence of the total conductivity, at 1000 ºC, of the three studied compositions as a function of the oxygen partial pressure with data from [12]

$$\left[O_i''\right] = \frac{\left[Zr_{Pr}^{\bullet}\right]}{2} \tag{10}$$

$$\mu_{V_O} = \frac{\sigma_i}{\left[V_O^{\bullet\bullet}\right]e} \tag{11}$$

$$\mu_{O_i} = \frac{\sigma_i}{\left[O_i''\right]e} \tag{12}$$

with Z and e, respectively, the defect charge and the electric charge of an electron, and σ_i the ionic conductivity value at the observed plateau.

Based on the experimental measurements of the electrical conductivity as a function of the oxygen partial pressure of Zr015 and Pr01 compositions (Figs. 3 and 4), where it can be seen a significant increase of the electrical conductivity when compared with the Stoich composition, it is evident in the strong effect of the non-stoichiometry. So, we can assume that variation of the value of ratio Pr/Zr from the unity will control the ionic conductivity value. Combining Eqs. (8), (9) and (10) and assuming the ionic conductivity given by the observed plateaus (Figs. 3 and 4), it is possible to calculate the oxygen vacancy and interstitial mobility, using the following equations:

$$\mu_{V_O^{\bullet\bullet}} = \frac{\sigma}{\left[Pr_{Zr}'\right].e} \tag{13}$$

$$\mu_{O_i''} = \frac{\sigma}{\left[Zr_{Pr}^{\bullet}\right].e} \tag{14}$$

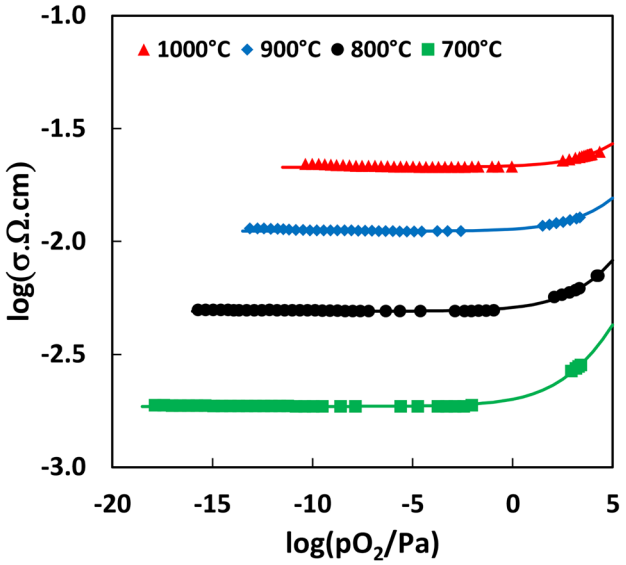

Fig.3 Dependence of the total electrical conductivity of Zr015 as a function of the oxygen partial pressure at different temperatures. Experimental data (dots) and fitting curve (lines)

As expected after the observation of the experimental data in Figs. 3 and 4, the calculated mobilities show that, in this material, the mobility of the interstitial oxygen is higher than the observed mobility for the oxygen vacancies.

Plotting the obtained mobility values for different temperatures on an Arrhenius-type chart, we can get the pre-exponential and the activation energy for these mobilities

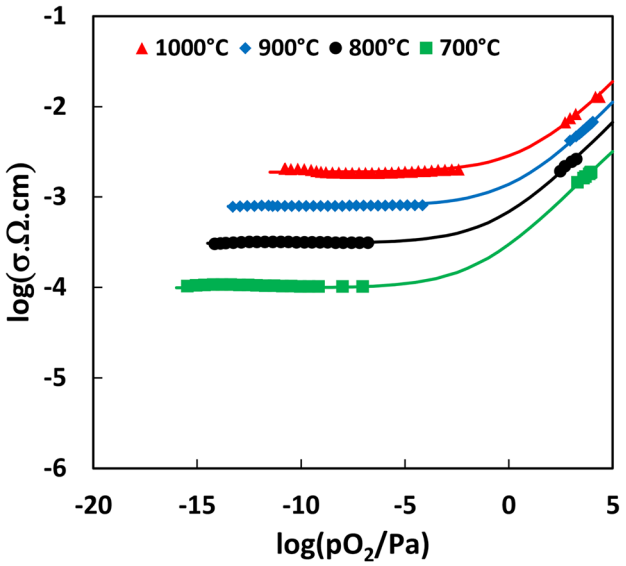

Fig. 4 Dependence of the total electrical conductivity of Pr01 as a function of the oxygen partial pressure at different temperatures. Experimental data (dots) and fitting curve (lines)

(Fig. 5), assuming the usual temperature dependency of the mobility for ionic (μ_i) and electronic (μ_e) defects, given by:

$$\mu_e = \frac{\mu_{e,0}}{T} exp\left(-\frac{E_{e,a}}{kT}\right) \quad (15)$$

$$\mu_i = \mu_{i,0} exp\left(-\frac{E_{i,a}}{kT}\right) \quad (16)$$

with $\mu_{e,0}$, $\mu_{i,0}$ and $E_{e,a}$, $E_{i,a}$, respectively the pre-exponential term and the activation energy for the electronic and ionic mobilities. It should be highlighted that interstitial oxygen has a higher mobility than oxygen vacancies, suggesting that the ionic conductivity of the Stoich composition is based on interstitial oxygen, in which the concentration of oxygen interstitial and vacancies should be equal because these defects are created by the intrinsic anti-Frenkel reactions (Eq. 1).

Using the Levenberg–Marquardt non-linear optimisation numerical method, available on DefChem software [25], one can fit the experimental conductivity results obtained for isothermal conditions by optimising the thermodynamic variables. The optimization routine was started over the Stoich composition, keeping constants the already calculated ionic mobilities μ_{Vo} and μ_{Oi}, leaving free the equilibrium constants K_{aF} and K_{Red} and also the *p*-type electronic mobility μ_p. This procedure allows us to get a good determination of the K_{aF} value because the ionic plateau only depends on this value and on the already calculated oxygen interstitial mobility. Fittings of *Pr01* and *Zr015* compositions were performed with only two free variables (K_{Red} and μ_p), and it was observed almost the same *p*-type mobility value for all three compositions for each temperature, and then, it was assumed that this *p*-type mobility should be composition-independent. Following these deductions, the variables μ_{Vo}, μ_{Oi} and K_{aF} were kept constant, and the numerical method was repeated to find K_{Red} for each of the three compositions.

It should be noted that the fitting of the *p*-type conductivity component can be achieved by optimising the value of the

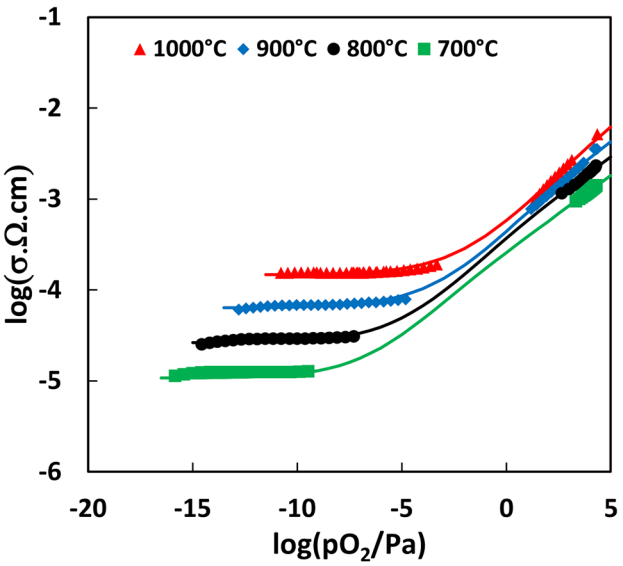

Fig. 6 Dependence of the total electrical conductivity of Stoich composition as a function of the oxygen partial pressure at different temperatures. Experimental data (dots) and fitting curve (lines)

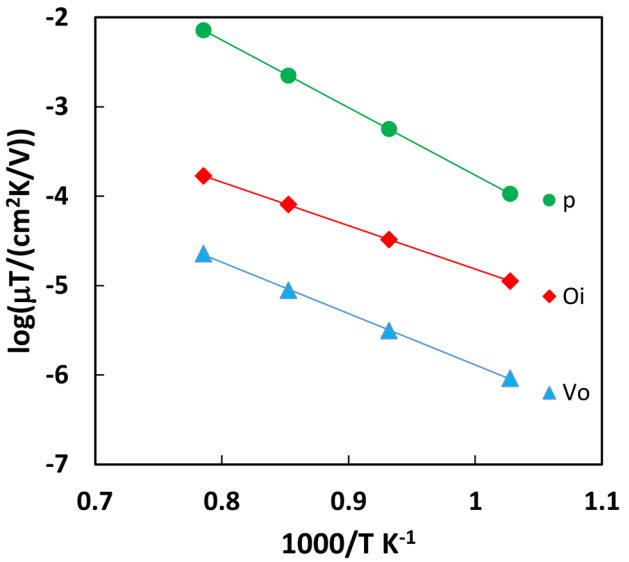

Fig. 5 Arrhenius-type plot of the calculated mobility of different defects

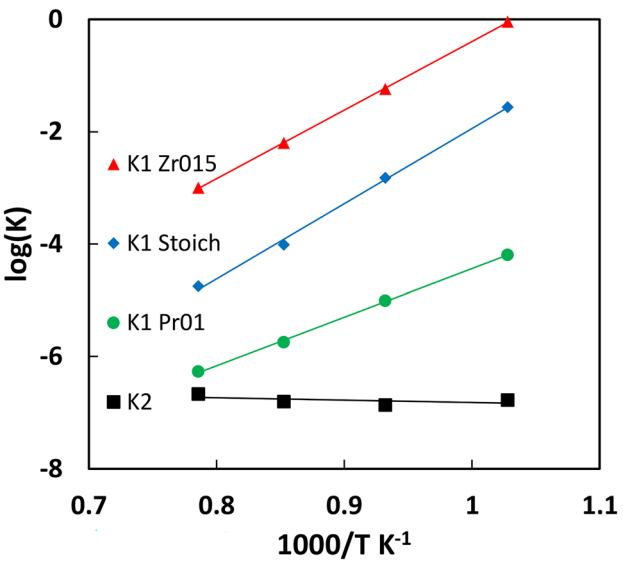

Fig. 7 Arrhenius-type plot of the calculated equilibrium constants of defects formation

Table 1 Relevant thermodynamic values obtained by fitting the experimental data

Composition	μ_{Vo}		μ_{Oi}		μ_p		K_{aF}		K_{Red}	
	μ_0	E_a/eV	μ_0	E_a/eV	μ_0	E_a/eV	K_0	E_a/eV	K_0	E_a
Stoich	728	1.14	1129	0.97	6.25×10^{-6}	1.5	2.23×10^{-6}	0.26	4.75×10^{-16}	-2.66
Zr015									2.40×10^{-13}	-2.43
Pr01									8.80×10^{-14}	-1.71

concentration of the electron holes (dependent of K_{Red}) or their mobility (μ_p), creating an undistinguishable dependence with these two parameters. Thus, should be necessary to use complementary methods to confirm these obtained values.

Fittings are present in Figs. 3, 4 and 6, and the Arrhenius-type plot of the obtained values for each temperature is represented in Figs. 5 and 7, with all relevant parameters in Table 1. The obtained results appear to be within the expected values for this kind of parameter, but in the absence of literature information, comparisons are not possible, except for the anti-Frenkel equilibrium constant, whose obtained value for the activation energy is close to 0.13 eV, as reported by Yu [28].

After obtaining all the thermodynamic parameters, it is possible to estimate the behaviour of these materials, such as the nature of the conductivity, as represented in Fig. 8, where the transport number is shown as a function of the oxygen partial pressure. In this figure, we can see that the Zr015, in addition to having the highest conductivity, also has the largest electrolyte domain.

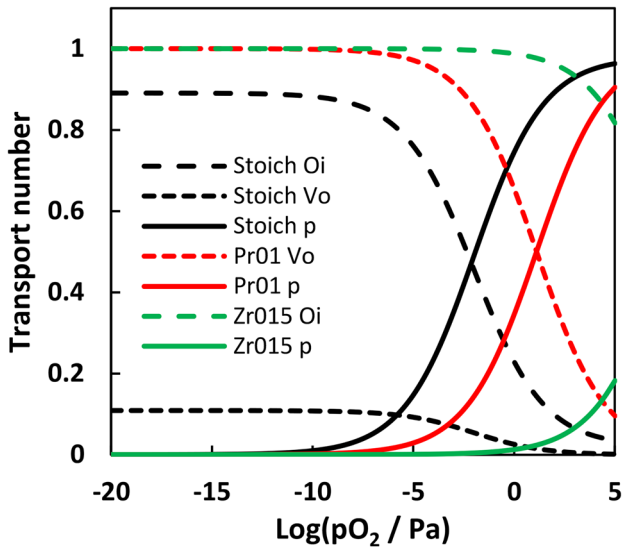

Fig. 8 Dependence of transport number as a function of the oxygen partial pressure for different compositions

Conclusions

The defect chemistry approach was used to evaluate the relevant thermodynamic parameters of the Pr_2O_3-ZrO_2 system, based on the conductivity behaviour as a function of the oxygen partial pressure. The observed plateau for reduction conditions was attributed to the ionic conductivity, and the increase of conductivity for high oxygen partial pressures was interpreted as a *p*-type electronic conductivity contribution.

The increase of the ionic conductivity for the nonstoichiometric compositions, according to the proposed defect chemistry model, was attributed to the ionic compensation of the defects ZrPr• and PrZr', respectively, by the formation of interstitials and oxygen vacancies.

Using the proposed defect chemistry model, the relevant thermodynamic parameters were obtained by fitting, using a non-linear optimisation numerical method. The mobility of oxygen vacancies and interstitial oxygen is accurately determined, assuming the concentration of these defects is fixed by the nonstoichiometric values, and using these values and the ionic conductivity of the stoichiometric composition, it was possible to get the equilibrium constant values of anti-Frenkel defect formation.

Applying the same procedure to several temperatures, it was possible to obtain the activation energies for the mobility of oxygen vacancies (1.12 eV) and interstitials (0.97 eV) and for the anti-Frenkel defect reaction (0.09 eV).

This work also shows that the use of numerical methods to fit experimental results with defect chemistry models can be an important tool for obtaining the relevant thermodynamic values of each system.

Acknowledgements This work was developed within the scope of the project proMetheus – Research Unit on Materials, Energy and Environment for Sustainability, FCT Ref. UID/05975/2020, financed by national funds through the FCT/MCTES. The work was supported partially by the subsidy from the Ministry of Education and Science allocated by the FRC CP RAS for the implementation of state assignment No.122040500071-0.

Funding Open access funding provided by FCT|FCCN (b-on).

Open Access This article is licensed under a Creative Commons Attribution 4.0 International License, which permits use, sharing, adaptation, distribution and reproduction in any medium or format, as long as you give appropriate credit to the original author(s) and the source, provide a link to the Creative Commons licence, and indicate if changes were made. The images or other third party material in this article are included in the article's Creative Commons licence, unless indicated otherwise in a credit line to the material. If material is not included in the article's Creative Commons licence and your intended use is not permitted by statutory regulation or exceeds the permitted use, you will need to obtain permission directly from the copyright holder. To view a copy of this licence, visit http://creativecommons.org/licenses/by/4.0/.

References

1. Zhang J, Lenser C, Menzler NH, Guillon O (2020) Comparison of solid oxide fuel cell (SOFC) electrolyte materials for operation at 500 °C. Solid State Ion 344:115138. https://doi.org/10.1016/j.ssi.2019.115138
2. Yeh T-H, Hsu W-C, Chou C-C (2005) Mechanical and electrical properties of ZrO 2 (3Y) doped with RENbO 4 (RE = Yb, Er, Y, Dy, YNd, Sm, Nd). Journal de Physique IV (Proceedings) 128:213–219. https://doi.org/10.1051/jp4:2005128032
3. Yoon S, Noh T, Kim W et al (2013) Structural parameters and oxygen ion conductivity of Y2O3–ZrO2 and MgO–ZrO2 at high temperature. Ceram Int 39:9247–9251. https://doi.org/10.1016/j.ceramint.2013.05.032
4. Xia C (2002) Microstructures, conductivities, and electrochemical properties of Ce0.9Gd0.1O2 and GDC–Ni anodes for low-temperature SOFCs. Solid State Ion 152–153:423–430. https://doi.org/10.1016/S0167-2738(02)00381-8
5. Li B, Wei X, Pan W (2010) Improved electrical conductivity of Ce0.9Gd0.1O1.95 and Ce0.9Sm0.1O1.95 by co-doping. Int J Hydrogen Energy 35:3018–3022. https://doi.org/10.1016/j.ijhydene.2009.07.002
6. Gao Z, Mogni LV, Miller EC et al (2016) A perspective on low-temperature solid oxide fuel cells. Energy Environ Sci 9:1602–1644. https://doi.org/10.1039/C5EE03858H
7. Lee D, Kim W, Chol S et al (2005) Characterization of ZrO co-doped with ScO and CeO electrolyte for the application of intermediate temperature SOFCs. Solid State Ion 176:33–39. https://doi.org/10.1016/j.ssi.2004.07.013
8. Yamamura H, Nishino H, Kakinuma K, Nomura K (2003) Electrical conductivity anomaly around fluorite–pyrochlore phase boundary. Solid State Ion 158:359–365. https://doi.org/10.1016/S0167-2738(02)00874-3
9. Nishino H, Yamamura H, Arai T et al (2004) Effect of cation radius ratio and unit cell free volume on oxide-ion conductivity in oxide systems with pyrochlore-type composition. J Ceram Soc Jpn 112:541–546. https://doi.org/10.2109/jcersj.112.541
10. Shlyakhtina AV, Pigalskiy KS (2019) Tolerance factor as the basic criterion in searching for promising oxygen-ion and proton conductors among Ln2-xDxM2O7-δ (Ln = La-Lu; M= Sn, Ti, Zr, Hf; D= Sr, Ca, Mg; x = 0, 0.1) 3+/4+ pyrochlores. Mater Res Bull 116:72–78. https://doi.org/10.1016/j.materresbull.2019.04.021
11. Lyskov NV, Shchegolikhin AN, Stolbov DN et al (2022) Study of oxygen-ion conductivity and luminescence in the ZrO2 – Nd2O3 system: impact of local heterogeneity. Electrochim Acta 403:139632. https://doi.org/10.1016/j.electacta.2021.139632
12. Shlyakhtina AV, Abrantes JCC, Gomes E et al (2016) Effect of Pr3+/Pr4+ ratio on the oxygen ion transport and thermomechanical properties of the pyrochlore and fluorite phases in the ZrO2–Pr2O3 system. Int J Hydrogen Energy 41:9982–9992. https://doi.org/10.1016/j.ijhydene.2016.02.152
13. Belov DAA, Shlyakhtina AVV, Abrantes JCC et al (2015) Electrochemical behavior of the pyrochlore- and fluorite-like solid solutions in the Pr2O3–ZrO2 system. Part I Solid State Ion 271:79–85. https://doi.org/10.1016/j.ssi.2014.09.035
14. Shamblin J, Tracy CL, Palomares RI et al (2018) Similar local order in disordered fluorite and aperiodic pyrochlore structures. Acta Mater 144:60–67. https://doi.org/10.1016/j.actamat.2017.10.044
15. Koohpayeh SM, Wen J-J, Trump BA et al (2014) Synthesis, floating zone crystal growth and characterization of the quantum spin ice Pr2Zr2O7 pyrochlore. J Cryst Growth 402:291–298. https://doi.org/10.1016/j.jcrysgro.2014.06.037
16. Alam J, Jana YM, Biswas AA (2016) Crystal-field study of magnetization and specific heat properties of frustrated pyrochlore Pr2Zr2O7. J Magn Magn Mater 416:391–400. https://doi.org/10.1016/j.jmmm.2016.05.030
17. Bonville P, Guitteny S, Gukasov A et al (2016) Magnetic properties and crystal field in Pr2Zr2O7. Phys Rev B 94:134428. https://doi.org/10.1103/PhysRevB.94.134428
18. Zhong F, Shi L, Zhao J et al (2018) Pyrochlore Pr2Zr2-xMxO7+δ (M = Al, Ga, In) solid-state electrolytes: defect-mediated oxygen hopping pathways and enhanced NO2 sensing properties. Sens Actuators B Chem 270:130–139. https://doi.org/10.1016/j.snb.2018.04.178
19. Zhong F, Zhao J, Shi L et al (2019) Pyrochlore Pr2Zr1.95In0.05O7+δ oxygen conductors: defect-induced electron transport and enhanced NO2 sensing performances. Electrochim Acta 293:338–347. https://doi.org/10.1016/j.electacta.2018.09.152
20. Fortuño-Morte M, Beltrán-Mir H, Cordoncillo E (2020) Study of the role of praseodymium and iron in an environment-friendly reddish orange pigment based on Fe doped Pr2Zr2O7: a multifunctional material. J Alloys Compd 845:155841. https://doi.org/10.1016/j.jallcom.2020.155841
21. Santos Veiga EL, Villafruela XV, Llorca J et al (2023) The catalytic activity of the Pr2Zr2−x FexO7±δ system for the CO oxidation reaction. J Am Ceram Soc 106:1369–1380. https://doi.org/10.1111/jace.18846
22. Zhong F, Yang S, Chen C et al (2022) Defect-induced pyrochlore Pr2Zr2O7 cathode rich in oxygen vacancies for direct ammonia solid oxide fuel cells. J Power Sources 520:230847. https://doi.org/10.1016/j.jpowsour.2021.230847
23. Bruggeman DAG (1935) Berechnung verschiedener physikalischer Konstanten von heterogenen Substanzen. I. Dielektrizitätskonstanten und Leitfähigkeiten der Mischkörper aus isotropen Substanzen. Ann Phys 416:636–664. https://doi.org/10.1002/andp.19354160705
24. Yang A, Wang C, Guo R, Huang Y (2010) Microstructure and electrical properties of porous PZT ceramics fabricated by different methods. J Am Ceram Soc 93:1984–1990. https://doi.org/10.1111/j.1551-2916.2010.03684.x
25. Abrantes JCC (2023) DefChem - Defect Chemistry Toolbox. https://doi.org/10.57910/ipvc-prometheus-defchem2023
26. Poulsen F (2000) Structure, Raman spectra and defect chemistry modelling of conductive pyrochlore oxides. Solid State Ion 135:595–602. https://doi.org/10.1016/S0167-2738(00)00417-3
27. Takamura H, Tuller HL (2000) Ionic conductivity of Gd2GaSbO7 – Gd2Zr2O7 solid solutions with structural disorder. Solid State Ion 134:67–73
28. Yu TH, Tuller HL (1996) Ionic conduction and disorder in the Gd2Sn2O7 pyrochlore system. Solid State Ion 86–88:177–182. https://doi.org/10.1016/0167-2738(96)00118-X
29. Kröger FA, Vink HJ (1956) Relations between concentrations of imperfections in crystalline solids. In: Seitz F, Turnbull D (eds) Solid State Physics. Academic Press, New York, pp 307–435

Publisher's Note Springer Nature remains neutral with regard to jurisdictional claims in published maps and institutional affiliations.